

Localization in musical steelpans

Petur Bryde¹ and L. Mahadevan^{1, 2, 3, *}

¹*Paulson School of Engineering and Applied Sciences,
Harvard University, Cambridge, MA 02138.*

²*Department of Physics, Harvard University, Cambridge, MA 02138.*

³*Department of Organismic and Evolutionary Biology,
Harvard University, Cambridge, MA 02138.*

The steelpan is a pitched percussion instrument that takes the form of a concave bowl with several localized dimpled regions of varying curvature. Each of these localized zones, called notes, can vibrate independently when struck, and produces a sustained tone of a well-defined pitch. While the association of the localized zones with individual notes has long been known and exploited, the relationship between the shell geometry and the strength of the mode confinement remains unclear. Here, we explore the spectral properties of the steelpan modeled as a vibrating elastic shell. To characterize the resulting eigenvalue problem, we generalize a recently developed theory of localization landscapes for scalar elliptic operators to the vector-valued case, and predict the location of confined eigenmodes by solving a Poisson problem. A finite element discretization of the shell shows that the localization strength is determined by the difference in curvature between the note and the surrounding bowl. In addition to providing an explanation for how a steelpan operates as a two-dimensional xylophone, our study provides a geometric principle for designing localized modes in elastic shells.

1. INTRODUCTION

When an elastic structure such as a beam, plate or shell of uniform curvature is struck, the resulting vibration quickly propagates as a wave through the entire system. In contrast, a flat portion of a shell surrounded by a region of higher curvature may support localized vibrational modes, i.e. stationary waves which are confined to a small subregion. This is the basic principle behind the steelpan, a pitched percussion instrument originating from Caribbean approximately a century ago [1]. It consists of a concave playing surface (referred to as the bowl) joined at the boundary to a cylindrical “skirt”, as shown in figure 1a. The playing surface has a number of flat or slightly concave regions which are able to vibrate independently, each with its own pitch (frequency) determined by its size and shape. These regions are called the notes of the pan, as each one is designed to resonate at a frequency corresponding to a certain note on the musical scale, thus making the steelpan a two-dimensional xylophone.

Steelpans were originally made from standard 55-gallon steel drums. The bottom face of the drum is hammered into a concave bowl shape and the notes are defined by locally raising and flattening the bowl, creating regions of lower curvature. A steelpan may have anywhere between three to upwards of 30 notes depending on the desired range. In most pans, the notes are arranged in concentric circles, with the inner notes either circular or elliptical while the outer notes resemble rounded rectangles (figure 1a). Part or all of the cylindrical side is retained as the skirt, which acts as an acoustic baffle, i.e. it prevents the cancellation of sound from the two sides of the bowl [1]. The steelpan and the crafting process have received considerable interest across multiple fields, including acoustics, mechanics and material science [2]. Studies of the steelpan have predominantly been experimental, and focus on either the materials science and metallurgy of the construction processes [3], or the measurements of spectra and mode shapes [1, 4–6] and of the sound field [7].

The pan is played by striking the notes with a soft-tipped mallet. However, the mechanism underlying the mode confinement in steelpan notes is still incomplete. Steelpan makers conventionally

* lmahadev@g.harvard.edu

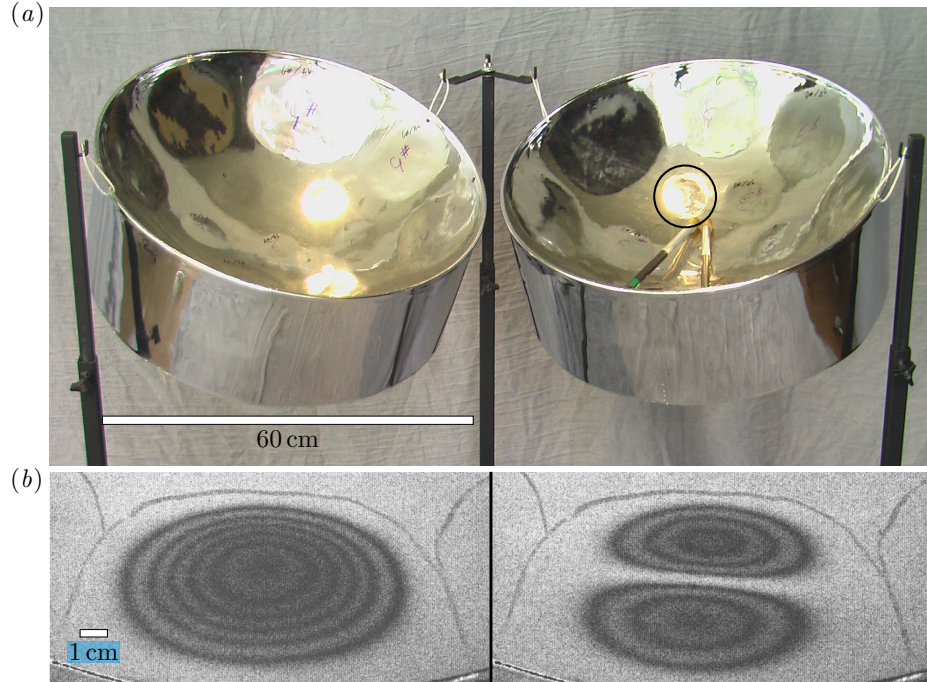


FIG. 1. (a) A “double second” steelpan with two types of note regions: The outer notes in the shape of rounded rectangles and elliptical inner notes. One of the inner notes is indicated by a black circle. Adapted from Vetter [8], ©2003 Roger Vetter, courtesy of the Grinnell College Musical Instrument Collection. (b) The first (left) and second (right) localized eigenmodes of a C₄ note on a “tenor” steelpan imaged using time-averaged TV holography. Adapted from Morrison [6] with permission from A.C. Morrison.

outline each note with chisel marks and mode confinement has sometimes been ascribed to this grooving process [2, 3]. This explanation was challenged by Maloney, Barlow, and Woodhouse, who proposed that mode confinement is a consequence of the steelpan geometry [5]. In a numerical and experimental modal analysis, they found that a flat circular note region on a hemispherical pan supports localized modes, suggesting that confinement is influenced by bowl curvature [5]. Later experimental studies using holographic interferometry reveal a number of normal modes that are completely localized to a single note region [6]; the mode shapes are qualitatively similar to those of a flat plate with the same dimensions. In general, the modes are designated by a pair of numbers (m, n) , where m is the number of radial nodal lines and n is the number of nodal lines perpendicular to the radial direction, e.g. the frequency of the fundamental, or $(0, 0)$ mode determines the pitch, and makers of the steelpan carefully control the geometry to achieve two or three harmonic overtones. To visualize this, Figure 1b shows experimental images of the $(0, 0)$ and $(0, 1)$ modes of a C₄ note, both displaying strong localization.

A similar mode confinement effect is observed in a related instrument, the musical saw, which consists of a strip of metal such as the blade of a regular handsaw. When bent into an ‘S-shape’, a number of localized vibrational modes emerge at the inflection line, where the non-vanishing principal curvature changes sign [9]. Recent work [10], quantified how the localization strength varies with the curvature gradient. Moreover, our analysis suggests that these classical confined modes are topologically protected, analogously to boundary modes in quantum-mechanical topological insulators.

Here, we characterize how localization in elastic shells arises from variations in the curvature of doubly curved shells, and characterize the strength of mode localization in the steelpan as a function of bowl curvatures. We model the steelpan as a thin linear elastic shell with an inhomogeneous cur-

vature, whose dynamics is governed by a set of coupled partial differential equations. To understand the vibrational properties of the system, we have to solve an eigenvalue problem for an idealized version of the pan geometry.

Here, instead we introduce an alternative approach based on a generalization of the localization landscape method of Filoche and Mayboroda [11]. Originally developed as a geometric alternative to explain Anderson localization [12] in quantum mechanical systems, one computes the landscape function associated with the system, whose peaks coincide with the possible localization regions. The landscape can be approximated by solving a single Poisson-like problem for the same operator, a computation which is considerably less expensive than solving the eigenvalue problem. The approach has been successfully used to analyze localized modes in various systems described by scalar equations [13–16]. Our generalization of the technique is applicable to elliptic systems of partial differential equations, which describe a wide variety of physical phenomena, including shell structures. We demonstrate the method for a steelpan-like shell with realistic note shapes.

The organization of the paper is as follows. In §2, the landscape theory for scalar PDE is reviewed and the vector landscape is introduced. In §3 we discuss the shell theory which we use to model the steelpan. In §4 describes the methodology of the modal analysis, including the simplified pan geometries and the numerical methods. The results are presented in §5.

2. VECTOR LOCALIZATION LANDSCAPE FOR ELLIPTIC SYSTEMS

(a) Review of localization landscape theory for scalar equations

Localization is a phenomenon exhibited by some vibrating systems where a standing wave is concentrated inside a small part of the domain and almost vanishing outside of it. As a result, a disturbance at one point of the medium need not propagate to the rest of the system. In the context of quantum mechanics, a localized wavefunction describes a particle which is confined to one region. A familiar example is localization due to a potential well, but the effect is observed in many less obvious cases. Localization may stem from the domain geometry, for instance due to a rough or irregular boundary, or when the system is composed of several weakly connected subdomains [17]. Confined modes can also arise in a disordered medium. The principal example of this is Anderson localization, where electron wavefunctions in a crystal are localized in the presence of a sufficiently rough or disordered potential [12].

To study localization in a general setting, we consider an elliptic partial differential operator L on a domain Ω in \mathbb{R}^n and the associated eigenvalue problem $Lw = \lambda w$. For instance, if $L = -\Delta + V$ is a Schrödinger operator where the potential V is piecewise constant with randomly chosen values, we obtain a model for Anderson localization. In general, it is not obvious whether any modes of L are localized or what the localization regions are. The recently developed localization landscape (LL) theory of Filoche and Mayboroda [11] provides a way to predict the confinement properties of low-frequency modes without solving the full eigenvalue problem. For a symmetric elliptic operator L acting on scalar functions, they defined the *localization landscape* as the function $\mathcal{L}: \Omega \rightarrow \mathbb{R}$ given by $\mathcal{L}(x) = \int_{\Omega} |G(x, y)| dy$, where G is the Green's function of L which satisfies the same boundary conditions as imposed in the eigenvalue problem. In systems which support low-frequency localized modes, the landscape has one or more peaks, coinciding with the localization regions, separated by valleys, where the eigenfunctions are necessarily small. This is made precise by the following inequality, satisfied by each eigenpair (λ, w) :

$$\frac{|w(x)|}{\|w\|_{L^\infty(\Omega)}} \leq \lambda \mathcal{L}(x), \quad \forall x \in \Omega. \quad (1)$$

The proof is remarkably short in the case when w is smooth (see [11]): from the definition of the

Green's function and the symmetry of L , we have

$$w(x) = \int_{\Omega} L_y G(x, y) w(y) dy = \int_{\Omega} G(x, y) L_y w(y) dy = \int_{\Omega} G(x, y) \lambda w(y) dy, \quad (2)$$

and thus

$$|w(x)| \leq \lambda \|w\|_{L^\infty(\Omega)} \int_{\Omega} |G(x, y)| dy. \quad (3)$$

If w is not necessarily smooth, we replace $w(x)$ by $\int_{\Omega} w(z) \varphi_{\varepsilon}(x - z) dz$ where φ_{ε} is a mollifier.

The inequality (1) says, roughly, that w is concentrated in the superlevel set $E(\lambda) = \{x \in \Omega \mid \mathcal{L}(x) \leq \lambda\}$. Note that $E(\lambda)$ may have several connected components, each encompassing a peak of the landscape \mathcal{L} . Therefore, the inequality (1) does not by itself guarantee that w is localized; instead it may be a linear combination of localized functions, each supported in a single connected component of $E(\lambda)$. However, numerical experiments [11, 14] have shown that typically, each eigenfunction is localized near a single peak of \mathcal{L} , with the following exceptions: (i) two eigenfunctions with nearly the same eigenvalue can share a peak, and (ii) an eigenfunction may be spread over two or more peaks that are sufficiently close together. This much stronger result has been made precise and shown rigorously for elliptic operators of the form $L = -\operatorname{div} A(x) \nabla + V(x)$ [16, Theorem 5.1].

It should be noted that when the Green's function is non-negative, as is the case when L is of second order, \mathcal{L} is precisely the solution u to the boundary value problem $Lu = 1$ on Ω , which simplifies its computation dramatically. For higher order operators, this is generally not the case; indeed, this condition fails even for the bilaplacian on certain domains [18]. However, if the negative part of G is relatively small, one can approximate the landscape by the solution to $Lu = 1$ and still obtain qualitatively correct results.

The localization landscape theory has found applications in semiconductor physics [13] and biochemistry [19] among other fields. However, many physical systems are described by systems of PDE, to which the existing landscape theory is not applicable. In particular, this includes the equations of linear elasticity and the shell equations considered in this paper. In the following section, we state an appropriate extension of the LL theory to elliptic systems by defining a vector-valued landscape \mathcal{L} and proving a generalization of the inequality (1).

(b) Generalization to elliptic systems

To simplify the exposition, we assume homogeneous Dirichlet boundary conditions throughout. In the following, $\|\cdot\|$ and $\langle \cdot, \cdot \rangle$ denote respectively the Euclidean norm and inner product of vectors or matrices considered as elements of $\mathbb{R}^{m \times n}$.

Let $\Omega \subset \mathbb{R}^n$ with $n \geq 2$ be a bounded domain and let L be a second order, symmetric elliptic operator which acts on vector-valued functions $\mathbf{u}: \Omega \rightarrow \mathbb{R}^m$ according to

$$(L\mathbf{u})_i = -\partial_{\alpha} \left(A_{ij}^{\alpha\beta} \partial_{\beta} u^j \right) + B_{ij} u^j, \quad (4)$$

where $A_{ij}^{\alpha\beta}$, B_{ij} are bounded, measurable functions. Since localization often arises in rough domains or for systems with highly irregular coefficients, we impose no further regularity restrictions on Ω or the coefficients. The operator should be understood in the weak sense, as follows: Let $H^1(\Omega)$ denote the usual Sobolev space of functions $f \in L^2(\Omega)$ with weak derivatives in $L^2(\Omega)$. The space $H_0^1(\Omega)$ is the completion in $H^1(\Omega)$ of $C_c^{\infty}(\Omega)$, the set of smooth functions with compact support. Functions in $H_0^1(\Omega)$ are said to satisfy Dirichlet boundary condition in the weak sense. The action of the operator L and the corresponding bilinear form a is given by

$$(L\mathbf{u}, \mathbf{v}) := a(\mathbf{u}, \mathbf{v}) = \int_{\Omega} A_{ij}^{\alpha\beta}(x) \partial_{\beta} u^j \partial_{\alpha} v^i + B_{ij} u^i v^j dx \quad (5)$$

for any $\mathbf{u}, \mathbf{v} \in \mathbf{H}_0^1 := (H_0^1(\Omega))^m$. For a vector field \mathbf{f} , we say that \mathbf{u} is a weak solution of the Dirichlet problem $L\mathbf{u} = \mathbf{f}$, $\mathbf{u}|_{\partial\Omega} = 0$ if $\mathbf{u} \in \mathbf{H}_0^1$ and

$$a(\mathbf{u}, \mathbf{v}) = (\mathbf{f}, \mathbf{v}) \quad \forall \mathbf{v} \in \mathbf{H}_0^1, \quad (6)$$

where $(\mathbf{f}, \mathbf{v}) = \int_{\Omega} \mathbf{f} \cdot \mathbf{v} \, dx$ denotes the inner product on $(L^2(\Omega))^m$.

The assumption that L is symmetric, meaning that $a(\mathbf{u}, \mathbf{v}) = a(\mathbf{v}, \mathbf{u})$ for all $\mathbf{u}, \mathbf{v} \in \mathbf{H}_0^1$, is equivalent to the condition

$$A_{ij}^{\alpha\beta} = A_{ji}^{\beta\alpha}, \quad B_{ij} = B_{ji}. \quad (7)$$

In addition, we assume that the bilinear form a is coercive on \mathbf{H}_0^1 , i.e. that for some $\mu > 0$,

$$a(\mathbf{u}, \mathbf{u}) \geq \mu \|\mathbf{u}\|_{\mathbf{H}_0^1}^2 = \mu \int_{\Omega} (\|\nabla \mathbf{u}\|^2 + \|\mathbf{u}\|^2) \, dx, \quad \forall \mathbf{u} \in \mathbf{H}_0^1. \quad (8)$$

This holds, for example, if the coefficients satisfy the strong ellipticity condition (see e.g. [20, chapter 13]),

$$\begin{aligned} A_{ij}^{\alpha\beta}(x) \xi_{\alpha}^i \xi_{\beta}^j &\geq c \|\boldsymbol{\xi}\|^2, \quad \forall \boldsymbol{\xi} \in \mathbb{R}^{m \times n}, \\ B_{ij}(x) \zeta^i \zeta^j &\geq 0, \quad \forall \boldsymbol{\zeta} \in \mathbb{R}^m, \end{aligned} \quad (9)$$

for some $c > 0$ (see also [21] for weaker but more technical conditions). Under these assumptions, there exists a unique weak solution to the boundary value problem (6) for any $\mathbf{f} \in [L^2(\Omega)]^m$. As an example, we note that our setting includes in particular the Lamé operator $L\mathbf{u} = -\partial_{\alpha}(H^{\alpha\beta\mu\nu}E(\mathbf{u})_{\mu\nu})$ of three-dimensional linear elasticity (see §3(c)), and the Naghdi shell operator of equation (29).

In continuum mechanics, one often encounters generalized eigenvalue problems of the form (cf. equation (33))

$$a(\mathbf{u}, \mathbf{v}) = \lambda m(\mathbf{u}, \mathbf{v}), \quad \forall \mathbf{v} \in \mathbf{H}_0^1. \quad (10)$$

where the bilinear form m is given by $m(\mathbf{u}, \mathbf{v}) = \int_{\Omega} \langle \mathbf{M}(x)\mathbf{u}(x), \mathbf{v}(x) \rangle \, dx$. We assume that the matrix-valued function \mathbf{M} is positive semidefinite for all x and with coefficients in $L^{\infty}(\Omega)$. Our goal is to obtain pointwise bounds for the generalized eigenfunctions in terms of integrals of the Green matrix of the system. We repeat here the definition of the Green matrix given in [21], specialized to our case. In the following, \mathbf{e}_k denotes the k th standard unit vector in \mathbb{R}^m and $B_r(y) := \{x \in \mathbb{R}^n \mid \|x - y\| < r\}$ is the open ball with center y and radius r .

Definition 2.1. We say that the matrix function $\mathbf{G}(x, y) = (G_{ij}(x, y))_{i,j=1}^m$ defined on $\{(x, y) \in \Omega \times \Omega \mid x \neq y\}$ is the Dirichlet Green matrix of L if the following holds:

1. For all $y \in \Omega$, $\mathbf{G}(\cdot, y)$ is locally integrable and satisfies $L\mathbf{G}(\cdot, y) = \delta_y I$ in the weak sense, i.e.

$$a(\mathbf{G}(\cdot, y)\mathbf{e}_k, \boldsymbol{\varphi}) = \varphi^k(y), \quad \forall \boldsymbol{\varphi} \in C_c^{\infty}(\Omega)^m. \quad (11)$$

2. For any $y \in \Omega$ and $r > 0$, $\mathbf{G}(\cdot, y) \in H^1(\Omega \setminus B_r(y))^{m \times m}$, and $\mathbf{G}(\cdot, y)$ vanishes on $\partial\Omega$ in the sense that for every $\zeta \in C_c^{\infty}(\Omega)$ satisfying $\zeta|_{B_r(y)} \equiv 1$ for some $r > 0$, we have

$$(1 - \zeta)\mathbf{G}(\cdot, y) \in H_0^1(\Omega \setminus B_r(y))^{m \times m} \quad (12)$$

3. For any $\mathbf{f} = (f^1, \dots, f^m)^T \in L^{\infty}(\Omega)^m$, the function $\mathbf{u} = (u^1, \dots, u^m)^T$ given by

$$\mathbf{u}(x) = \int_{\Omega} \mathbf{G}(x, y)\mathbf{f}(y) \, dy$$

is the unique weak solution in \mathbf{H}_0^1 to $L\mathbf{u} = \mathbf{f}$.

We note that since L is assumed to be symmetric, \mathbf{G} satisfies the symmetry relation $\mathbf{G}(x, y) = \mathbf{G}(y, x)^T$. Assume that (λ, \mathbf{w}) is an eigenpair, i.e. a solution of (10), and assume moreover that $\mathbf{w} \in L^\infty(\Omega)^m$. Then $\lambda \mathbf{M} \mathbf{w} \in L^\infty(\Omega)^m$ and from property (iii) of Definition (2.1), it follows that the function \mathbf{u} defined by

$$\mathbf{u}(x) = \int_{\Omega} \mathbf{G}(x, y) \lambda \mathbf{M}(y) \mathbf{w}(y) dy$$

is in \mathbf{H}_0^1 and satisfies $L\mathbf{u} = \lambda \mathbf{M} \mathbf{w}$ in the sense of distributions. By uniqueness of solutions, it follows that $\mathbf{u} = \mathbf{w}$. Interchanging the roles of x and y and using the symmetry property of the Green's matrix, we find for the i th component of \mathbf{w} :

$$w^i(y) = \lambda \int_{\Omega} \langle \mathbf{G}(y, x) \mathbf{M}(x) \mathbf{w}(x), \mathbf{e}_i \rangle dx = \lambda \int_{\Omega} \langle \mathbf{M}(x) \mathbf{w}(x), \mathbf{G}(x, y) \mathbf{e}_i \rangle dx.$$

Let $\mathbf{M}^{\frac{1}{2}}$ denote the unique positive semidefinite square root of \mathbf{M} . From the Cauchy–Schwarz inequality in \mathbb{R}^m , we have

$$\begin{aligned} |w^i(y)| &\leq \lambda \int_{\Omega} |\langle \mathbf{M}^{\frac{1}{2}}(x) \mathbf{w}(x), \mathbf{M}^{\frac{1}{2}} \mathbf{G}(x, y) \mathbf{e}_i \rangle| dx \\ &\leq \lambda \int_{\Omega} \|\mathbf{M}^{\frac{1}{2}}(x) \mathbf{w}(x)\| \|\mathbf{M}^{\frac{1}{2}}(x) \mathbf{G}(x, y) \mathbf{e}_i\| dx \\ &\leq \lambda \|\mathbf{M}^{\frac{1}{2}} \mathbf{w}\|_{L^\infty(\Omega)} \int_{\Omega} \|\mathbf{M}^{\frac{1}{2}}(x) \mathbf{G}(x, y) \mathbf{e}_i\| dx. \end{aligned}$$

Defining the *vector landscape* $\mathcal{L}: \Omega \rightarrow \mathbb{R}^m$ as the vector field with components

$$\mathcal{L}^i(y) := \int_{\Omega} \|\mathbf{M}^{\frac{1}{2}} \mathbf{G}(x, y) \mathbf{e}_i\| dx. \quad (13)$$

we obtain the following generalization of the scalar inequality (1):

Proposition 2.1. *Assume a Dirichlet Green's matrix \mathbf{G} exists for L and that \mathbf{w} is a bounded eigenfunction satisfying (10). Then*

$$\left(\|\mathbf{M}^{\frac{1}{2}} \mathbf{w}\|_{L^\infty(\Omega)} \right)^{-1} |w^i(x)| \leq \lambda \mathcal{L}^i(x), \quad x \in \Omega. \quad (14)$$

where \mathcal{L} is defined in equation (13).

The interpretation is similar to the scalar case: The inequality states that each component of w^i is concentrated in the superlevel set $E^i(\lambda) = \{x \in \Omega \mid \mathcal{L}^i(x) \leq \lambda\}$ of the corresponding component of the vector landscape. Our numerical experiments experiments (§5(b)) suggest that, at least for some systems, w^i will in fact be localized near a single peak of \mathcal{L}^i , as in the scalar case. We conjecture that an analogue of theorem 5.1 in [16] holds also for the vector landscape.

As a concrete example, consider the equations of three-dimensional linear elasticity, equation (28). Then $\mathbf{M} = \mathbf{I}$ is the identity matrix, and the vector landscape yields a simple upper bound on the norm of the displacement \mathbf{U} :

$$\|\mathbf{U}(x)\| \leq \lambda \|\mathcal{L}(x)\|, \quad \mathcal{L}^i(x) = \int_{\Omega} \|\mathbf{G}(x, y) \mathbf{e}_i\| dx, \quad (15)$$

where the eigenfunction has been normalized so that $\|\mathbf{U}\|$ has L^∞ -norm 1. In the remainder of the paper, we will consider the Naghdi eigenvalue problem, equation (33), for which \mathbf{M} is the diagonal matrix $\mathbf{M} = \text{diag}(1, 1, 1, 0, 0)$, and we again obtain an upper bound on the norm of the displacement:

$$\|\mathbf{u}(x)\| \leq \lambda \|\mathcal{L}(x)\|, \quad \mathcal{L}^i(x) = \int_{\Omega} \|\tilde{\mathbf{G}}(x, y) \mathbf{e}_i\| dx \quad (16)$$

where $\tilde{\mathbf{G}}$ is the upper-left 3×3 submatrix of \mathbf{G} and $\mathbf{e}_i \in \mathbb{R}^3$. Finally, we note that the statement of Proposition 2.1 is easily modified to account for different boundary conditions, namely by replacing the Dirichlet Green's matrix with one satisfying the same boundary conditions as \mathbf{w} .

3. THE ELASTIC SHELL MODEL

To apply our generalization of the localization landscape to the steelpan modeled mathematically as a thin elastic shell. The mechanics of three-dimensional structures which are thin in one direction in comparison with the other two are simplified versions of the 3D equations of continuum mechanics, and apply to the two-dimensional problem of finding the deformation of the midsurface. Shell theories can be seen as a generalization of the more familiar plate theories, which model flat bodies, to structures which may be curved in their rest state. Like plates, shells are much weaker to bending (i.e. isometric deformations) than they are to stretching and shearing. For shells, however, the membrane (stretching) strains are generally coupled to the bending and shearing strains due to the curvature of the midsurface. This has a dramatic effect on the mechanics, allowing shells to resist applied loads more effectively. The curvature of the midsurface also complicates the analysis: In contrast to plates, the equations describing in-surface and transverse displacements are coupled, and one must generally work in curvilinear coordinates. Apart from exceptional cases, the equations of shell theory can only be solved numerically.

There are a number of different shell theories, each based on different physical assumptions; see for example [22] for an overview. Here we use a specific model known as the Naghdi shell model [23], which allows for extensional and shear deformations of the mid-surface, as well shear and bending deformations transverse to the mid-surface. These kinematical assumptions are the same as the well-known Reissner–Mindlin model for thin plates [22], to which the Naghdi model reduces in the special case of a flat midsurface. The choice of model is motivated by ease of computation: shearable theories such as the Naghdi model require only H^1 -conforming finite elements methods, which are relatively simple to implement and are available in many free software packages. This should be contrasted with models that do not allow for transverse shear which give rise to weak formulations with solutions in H^2 , and thus call for more complicated H^2 -conforming or discontinuous Galerkin methods.

We start with a derivation of the Naghdi equations for completeness, following [22], leading directly to the equations of motion in weak form, required to apply the finite element method. Since our goal is modal analysis of the steelpan, we limit the discussion to the linearized theory and clamped boundary conditions. For simplicity, we consider only the case of an isotropic, homogeneous material of constant thickness.

(a) Differential geometry of a deforming shell

We adopt the convention that Latin indices denote components of (2D) surface tensors and take the values $\{1, 2\}$, while Greek indices denote components of 3D tensors and take the values $\{1, 2, 3\}$; repeated indices are summed as usual. The shell is defined as a three-dimensional (3D) slender elastic body specified by a reference surface \mathcal{S} , representing the midsurface of the undeformed configuration, and a constant thickness h , which is assumed small compared to the lateral dimensions and radius of curvature of the shell. The midsurface is parametrized by a map $\mathbf{X}_0 : \Omega_0 \rightarrow \mathbb{R}^3$ where the *reference domain* Ω_0 is a bounded domain in \mathbb{R}^2 . At any point on the midsurface, the vectors $\mathbf{e}_i = \partial_i \mathbf{X}_0$ are linearly independent, and form the covariant basis for the tangent plane. We also define the unit normal vector $\mathbf{e}_3 = (\mathbf{e}_1 \times \mathbf{e}_2) / \|\mathbf{e}_1 \times \mathbf{e}_2\|$. The undeformed shell body is then parametrized by

$$\mathbf{R}_0(\xi^1, \xi^2, \xi^3) = \mathbf{X}_0(\xi^1, \xi^2) + \xi^3 \mathbf{e}_3(\xi^1, \xi^2), \quad (\xi^1, \xi^2, \xi^3) \in \Omega := \Omega_0 \times \left[-\frac{h}{2}, \frac{h}{2}\right], \quad (17)$$

where ξ^α are the local 3D coordinates within the material. We follow the usual convention of denoting components of tensors with respect to the covariant basis by superscripts; we call these the *contravariant* components. Subscript indices indicate *covariant components*, which are components with respect to the contravariant basis $(\mathbf{e}^1, \mathbf{e}^2)$, defined by the relation $\mathbf{e}^i \cdot \mathbf{e}_j = \delta^i_j$.

The first fundamental form \mathbf{a} and second fundamental form \mathbf{b} of the reference midsurface have the covariant components

$$a_{ij} = \partial_i \mathbf{X}_0 \cdot \partial_j \mathbf{X}_0, \quad b_{ij} = \mathbf{e}_3 \cdot \partial_i \partial_j \mathbf{X}_0. \quad (18)$$

The reference area element of the surface is $dA = \sqrt{\det(\mathbf{a})} d\xi^1 d\xi^2$. Indices of midsurface tensors are raised and lowered using \mathbf{a} . For example, the components of a vector $\mathbf{V} = V^i \mathbf{e}_i = V_i \mathbf{e}^i$ are related by $V_i = a_{ij} V^j$. The 3D reference metric tensor $g_{\alpha\beta} = \partial_\alpha \mathbf{R}_0 \cdot \partial_\beta \mathbf{R}_0$ has a simple expression in terms of the fundamental forms:

$$g_{ij} = a_{ij} - 2\xi^3 b_{ij} + (\xi^3)^2 b_i^k b_{kj}, \quad g_{i3} = 0, \quad g_{33} = 1. \quad (19)$$

Finally, covariant derivatives of midsurface tensors are defined in terms of the Christoffel symbols $\Gamma_{ij}^k = \partial_i \mathbf{e}_j \cdot \mathbf{e}^k$ of the reference surface, so that e.g.,

$$\nabla_i V^j = \partial_i V^j + \Gamma_{ik}^j V^k, \quad \nabla_i V_j = \partial_i V_j - \Gamma_{ij}^k V_k. \quad (20)$$

for the vector field \mathbf{V} .

(b) Kinematics

We let $\mathbf{U}(\xi)$ be the displacement of the material point of the shell which is initially at $\mathbf{R}_0(\xi)$ (the deformed position is then $\mathbf{R} = \mathbf{R}_0 + \mathbf{U}$). To reduce the dimensionality of the model, we make the Reissner–Mindlin kinematic assumption, which specifies the displacement \mathbf{U} of an arbitrary point of the shell in terms of two vector fields defined on the midsurface: A displacement vector field \mathbf{u} and a rotation (θ_1, θ_2) of the unit normal. Specifically, we assume that the displacement takes the form

$$\mathbf{U} = u^\alpha \mathbf{e}_\alpha + \xi^3 \theta^i \mathbf{e}_i. \quad (21)$$

In words, the assumption states that a material line initially normal to the midsurface remains straight and unstretched in the deformed state, but may be translated and rotated. We see that \mathbf{u} is the translation of the midsurface while θ_i are the rotations of the material line around the axes defined by the tangent vectors \mathbf{e}_i (see figure 2).

The full nonlinear strain tensor is defined by $E_{\alpha\beta} = (1/2)(\bar{g}_{\alpha\beta} - g_{\alpha\beta})$, where $\bar{g}_{\alpha\beta} = \partial_\alpha \mathbf{R} \cdot \partial_\beta \mathbf{R}$ is the metric of the deformed configuration. To leading order in variations along the thickness (i.e. ξ^3), we obtain

$$\begin{aligned} E_{ij} &= \varepsilon_{ij} + \xi^3 C_{ij} + \mathcal{O}((\xi^3)^2), \\ E_{i3} &= S_i, \\ E_{33} &= 0, \end{aligned} \quad (22)$$

where ε_{ij} is the in-plane strain, C_{ij} is the curvature or bending strain and S_i is the transverse shear strain, given by

$$\varepsilon_{ij} = \frac{1}{2} (\nabla_i u_j + \nabla_j u_i) - b_{ij} u_3, \quad (23a)$$

$$C_{ij} = \frac{1}{2} (\nabla_i \theta_j + \nabla_j \theta_i - b_i^k \nabla_j u_k - b_j^k \nabla_i u_k) + b_i^k b_{kj} u_3, \quad (23b)$$

$$S_i = \frac{1}{2} (\theta_i + \partial_i u_3 + b_i^k u_k), \quad (23c)$$

as depicted in figure 2b.

Remarks. (i) In the case of a flat plate, the second fundamental form b_{ij} vanishes and equations (22)–(23) reduce to the usual strain tensor of the Reissner–Mindlin plate model. Note that in

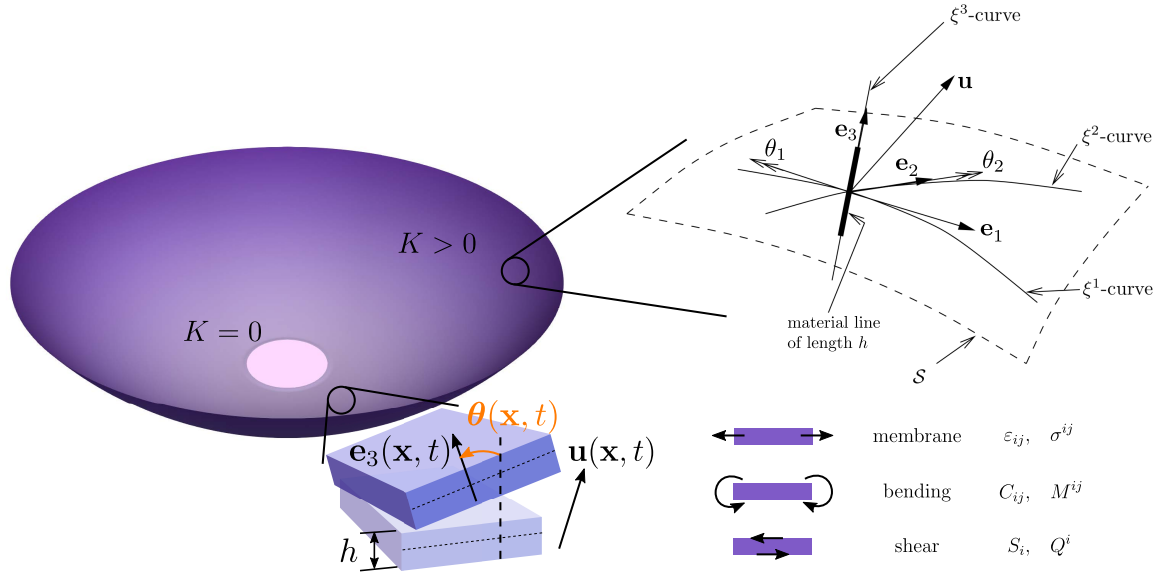


FIG. 2. A simplified model of the steelpan as a thin elastic shell in the shape of a hemispherical bowl (positive Gaussian curvature K) with a flat central note ($K = 0$). In the Naghdi shell theory, the deformations are described by the midsurface displacement \mathbf{u} and the rotation $\boldsymbol{\theta}$ of material lines which are orthogonal to the midsurface in the undeformed configuration. The equations of motion (written in weak form in equation (29) and in strong form in equation (35)) take into account the elastic energy associated with membrane (stretching), bending and shear strains (23) and stresses (34) (adapted from Shankar et al. [10], and Chapelle and Bathe [22]).

this case, the in-plane membrane strain tensor ε_{ij} depends only on the in-plane displacement u_i and is uncoupled from the bending and shearing strains. (ii) A displacement field of the form given in equation (21) where $\theta_i = -\nabla_i u_3 - b_i^k u_k$ is said to satisfy the Kirchhoff–Love kinematic assumption. It is stronger than the Reissner–Mindlin hypothesis as it imposes that a material line which is initially normal to the midsurface remains normal in the deformed state as well. From equation (23c), this is equivalent to the transverse shear strain S_i vanishing. (iii) If the displacement field satisfies the Kirchhoff–Love assumption and the shell is flat ($a_{ij} = \delta_{ij}$, $b_{ij} = 0$), we obtain the Kirchhoff–Love plate model.

(c) Governing equations

We derive the dynamical Naghdi equations starting from the continuum mechanics of the three-dimensional shell body. The constitutive relation for the 3D stress tensor $\Sigma^{\alpha\beta} = H^{\alpha\beta\mu\nu} E_{\mu\nu}$ involves the elastic tensor (for an isotropic material)

$$H^{\alpha\beta\mu\nu} = \frac{Y}{2(1+\nu)} \left[g^{\alpha\mu} g^{\beta\nu} + g^{\alpha\nu} g^{\beta\mu} + \frac{2\nu}{(1-2\nu)} g^{\alpha\beta} g^{\mu\nu} \right], \quad (24)$$

where Y and ν are the Young's modulus and Poisson's ratio of the material, respectively. Using the expression for the 3D metric tensor, equation (19), along with the standard additional assumption that the normal stress Σ^{33} vanishes everywhere, we get

$$\Sigma^{ij} = \tilde{\mathcal{A}}^{ijkl} E_{kl}, \quad \Sigma^{i3} = \frac{1}{2} \tilde{\mathcal{B}}^{ij} E_{j3}, \quad (25)$$

with the reduced elastic tensors

$$\tilde{\mathcal{A}}^{ijkl} = \frac{Y}{2(1+\nu)} \left(g^{ik}g^{j\ell} + g^{i\ell}g^{kj} + \frac{2\nu}{(1-\nu)}g^{ij}g^{k\ell} \right), \quad \tilde{\mathcal{B}}^{ij} = \frac{2Y}{1+\nu}g^{ij}. \quad (26)$$

Newton's second law for the 3D shell reads

$$\rho \partial_t^2 \mathbf{U} = \nabla \cdot \boldsymbol{\Sigma} + \mathbf{F}, \quad (27)$$

where ρ is the mass density and $\mathbf{F} = F^\alpha \mathbf{e}_\alpha$ is an external force density on the shell. To obtain a weak form of the equation, suitable for the finite element method, we introduce a test vector field \mathbf{V} which satisfies the same kinematic assumptions as \mathbf{U} , i.e., $\mathbf{V} = v^\alpha \mathbf{e}_\alpha + \xi^3 \eta^i \mathbf{e}_i$, and vanishes on the lateral boundary (corresponding to $(\xi^1, \xi^2) \in \partial\Omega_0$) where the displacement boundary condition $\mathbf{U} = \mathbf{0}$ is prescribed.

Taking the inner product of equation (27) with \mathbf{V} and integrating by parts, we obtain

$$\int_{\Omega} dV \rho \partial_t^2 \mathbf{U} \cdot \mathbf{V} + \int_{\Omega} dV \boldsymbol{\Sigma}(\mathbf{U}) : \mathbf{E}(\mathbf{V}) = \int_{\Omega} dV \mathbf{F} \cdot \mathbf{V} + \int_{\partial\Omega} dS (\boldsymbol{\Sigma}(\mathbf{U}) \cdot \hat{\mathbf{\nu}}) \cdot \mathbf{V}. \quad (28)$$

where $dV = \sqrt{\det(\mathbf{g})} d\xi^1 d\xi^2 d\xi^3$ is the volume element and $\hat{\mathbf{\nu}}$ is the unit outward normal along the boundary of the 3D shell, with dS the boundary area element. The last term of equation (28) represents the effect of boundary tractions, and can be divided into integrals over the upper and lower faces of the shell (corresponding to $\xi^3 = \pm h/2$), and an integral over the lateral faces. The upper and lower faces of the shell are free, meaning that the traction $\boldsymbol{\Sigma}(\mathbf{U}) \cdot \hat{\mathbf{\nu}}$ vanishes. Moreover, $\mathbf{V} = 0$ on the lateral faces as previously noted. Therefore, the last term of equation (28) vanishes for this choice of boundary conditions.

Upon expanding the second term on the left-hand side of equation (28), and integrating over the thickness of the shell (to leading order in ξ^3 , conversely h), we obtain the dynamic Naghdi equations in weak form:

$$\begin{aligned} \int_{\Omega_0} dA \rho h \partial_t^2 u_\alpha v^\alpha + \int_{\Omega_0} dA h \mathcal{A}^{ijkl} \left[\varepsilon_{ij}(\mathbf{u}) \varepsilon_{k\ell}(\mathbf{v}) + \frac{h^2}{12} C_{ij}(\mathbf{u}, \boldsymbol{\theta}) C_{k\ell}(\mathbf{v}, \boldsymbol{\eta}) \right] \\ + \int_{\Omega_0} dA h \mathcal{B}^{ij} S_i(\mathbf{u}, \boldsymbol{\theta}) S_j(\mathbf{v}, \boldsymbol{\eta}) = \int_{\Omega_0} dA h F_\alpha v^\alpha, \end{aligned} \quad (29)$$

where $dA = \sqrt{\det(\mathbf{a})} d\xi^1 d\xi^2$ is the area element on the midsurface and \mathcal{A}, \mathcal{B} are the restrictions of the elastic tensors $\tilde{\mathcal{A}}, \tilde{\mathcal{B}}$ onto the midsurface, i.e.,

$$\mathcal{A}^{ijkl} = \frac{Y}{2(1+\nu)} \left(a^{ik}a^{j\ell} + a^{i\ell}a^{jk} + \frac{2\nu}{(1-\nu)}a^{ij}a^{k\ell} \right), \quad \mathcal{B}^{ij} = \frac{2Y}{(1+\nu)}a^{ij}. \quad (30)$$

It remains to specify an appropriate space of functions \mathcal{V} in which to seek the solution. Since the weak form of Naghdi's equations, equation (29), involves only first order derivatives, this will be a subspace of the Sobolev space $(H^1(\Omega_0))^5$. In order to impose clamped (homogeneous Dirichlet) boundary conditions, we take $\mathcal{V} := (H_0^1(\Omega_0))^5$, the subspace of functions which vanish at the boundary.

For convenience, we will use the shorthand $u = (\mathbf{u}, \boldsymbol{\theta})$, $v = (\mathbf{v}, \boldsymbol{\eta})$, and let k_m , k_b and k_s denote the membrane, bending and shear terms of equation (29):

$$\begin{aligned} k_m(u, v) &= \int_{\Omega_0} dA h \mathcal{A}^{ijkl} \varepsilon_{ij}(\mathbf{u}) \varepsilon_{k\ell}(\mathbf{v}) \\ k_b(u, v) &= \int_{\Omega_0} dA \mathcal{A}^{ijkl} \frac{h^3}{12} C_{ij}(\mathbf{u}, \boldsymbol{\theta}) C_{k\ell}(\mathbf{v}, \boldsymbol{\eta}) \\ k_s(u, v) &= \int_{\Omega_0} dA h \mathcal{B}^{ij} S_i(\mathbf{u}, \boldsymbol{\theta}) S_j(\mathbf{v}, \boldsymbol{\eta}). \end{aligned} \quad (31)$$

Lastly, we define the bilinear forms

$$\begin{aligned} m(u, v) &= \int_{\Omega_0} dA \rho h u_\alpha v^\alpha, \\ k(u, v) &= k_m(u, v) + k_b(u, v) + k_s(u, v), \end{aligned} \quad (32)$$

which we call the mass and stiffness form, respectively. With this notation in place, the eigenvalue problem associated with (29) can be stated succinctly as: Find pairs (ω^2, u) with $\omega^2 > 0$, $u = (\mathbf{u}, \boldsymbol{\theta}) \in \mathcal{V} := (H_0^1(\Omega_0))^5$ so that

$$k(u, v) = \omega^2 m(u, v) \quad \text{for all } v \in \mathcal{V}. \quad (33)$$

For completeness, we mention that the Naghdi equations can also be written as a boundary value problem in strong form as follows: Define the in-plane stress $\boldsymbol{\sigma}$, bending moment \mathbf{M} and transverse shear stress \mathbf{Q} by

$$\begin{aligned} \sigma^{ij} &= h \mathcal{A}^{ijkl} \varepsilon_{kl} \\ M^{ij} &= \frac{h^3}{12} \mathcal{A}^{ijkl} C_{kl} \\ Q^i &= \frac{h}{2} \mathcal{B}^{ij} S_j. \end{aligned} \quad (34)$$

Then the weak form (29) is formally equivalent to the following system of equations:

$$\begin{aligned} \rho h \partial_t^2 u^i &= \nabla_j \sigma^{ij} - b_j^i Q^j - \nabla_j (b_k^i M^{kj}) + h F^i, \quad i = 1, 2, \\ \rho h \partial_t^2 u^3 &= \nabla_i Q^i + b_{ij} \sigma^{ij} - b_i^k b_{kj} M^{ij} + h F^3, \\ 0 &= Q^i - \nabla_j M^{ij}, \quad i = 1, 2. \end{aligned} \quad (35)$$

Remarks. (i) We note that in equation (29), the bending term k_b is of higher order in the thickness h compared to the stretching and shearing terms, a general feature of shell models [22]. In the limit of small thickness, modes with vanishing membrane and shear strains are energetically favorable. In the linear theory, these pure-bending modes are characterized by $\boldsymbol{\varepsilon} = \mathbf{0}$, and $\boldsymbol{\theta} = -(\nabla u_3 + \mathbf{b} \cdot \mathbf{u})$. Existence of pure-bending displacements depends on the boundary conditions as well as the midsurface reference geometry, in particular the sign of the Gaussian curvature $K = \det(\mathbf{b})/\det(\mathbf{a})$ [22]. Isometric bending deformations are well understood for surfaces where K has a constant sign, but less is known for surfaces of mixed type where K changes sign. (ii) If we replace the Reissner–Mindlin kinematic assumptions with the stronger Kirchhoff–Love assumption, we obtain instead the weak form of Koiter’s equations [22]. (iii) In the absence of curvature (i.e. $b_{ij} = 0$), the variational problem of equation (29) splits into two decoupled equations: a membrane problem for the in-plane displacement (u_1, u_2) and the remaining variables $(u_3, \boldsymbol{\theta})$ satisfy the Reissner–Mindlin plate equations. If we instead make the Kirchhoff–Love kinematic assumption, which for a flat plate states that $\theta_i = -\nabla_i u_3$, then the normal displacement u_3 satisfies a simple bending equation. If we choose orthonormal coordinates so that $a_{ij} = \delta_{ij}$, the equation is

$$\rho h \partial_t^2 u^3 + B \nabla^4 u^3 = h F^3 \quad (36)$$

where $B = Y h^3 / [12(1 - \nu^2)]$. This is most easily seen from the strong form equations (35).

4. STEELPAN MODEL AND NUMERICAL SIMULATIONS

(a) Numerical methods

We discretize the Naghdi eigenvalue problem, equation (33), in space using the finite element method. As previously mentioned, the weak form of the Naghdi equations admits solutions in H^1 .

However, it is well known that standard H^1 -conforming finite element methods suffer from numerical locking when applied to shell models, which leads to overstiff behavior unless a very fine mesh is used. Several approaches to alleviate locking have been proposed, see [24, 25] and references therein. While no method has been rigorously shown to be locking free for all problems, numerical tests suggest that many of the known methods can successfully treat locking in the Naghdi model. Following [25], we use a high-order partial selective reduced integration (PSRI) method, a variation of the technique introduced in [24]. This method was shown in [24] to converge uniformly with respect to the shell thickness under some restrictive assumptions on the coefficients in the Naghdi model. In the PSRI approach, second-order Lagrange finite elements augmented by cubic bubble functions are used for the displacements (u_α), and second-order Lagrange finite elements are used for the rotations (θ_i). The stiffness form k in equation (33) is modified by splitting the membrane term k_m and shear term k_s into a weighted sum of two contributions, one of which is computed with a reduced integration. That is, we write k_m as

$$\alpha \int_{\Omega_0} dA h \mathcal{A}^{ijkl} \varepsilon_{ij}(\mathbf{u}) \varepsilon_{kl}(\mathbf{v}) + (1 - \alpha) \int_{\Omega_0} dA h \mathcal{A}^{ijkl} \varepsilon_{ij}(\mathbf{u}) \varepsilon_{kl}(\mathbf{v})$$

and compute the second integral using a reduced quadrature rule of order 2. The shear term k_s is similarly modified. The splitting parameter α is chosen as $h^2/\delta^2 \approx 0.05$ where δ is a typical element circumradius for the mesh, as suggested in [25]. Discretizing equation (33) in the manner just described yields a (generalized) matrix eigenvalue problem which we solve using the SLEPc implementation of the Krylov-Schur algorithm [26]. The numerical method just described is implemented in a custom code based on the FEniCS-Shells library [27] and using the open-source finite element computing platform FEniCS [28]. The code is included in the supplementary material [29].

(b) Steelpan model and numerical experiments

In a real steelpan, the crafting process introduces inhomogeneities in the thickness and material properties. While these effects may influence the sound of the instrument, as we show, they are not necessary for studying mode localization and can be neglected for our purposes. For the same reason, the skirt of the pan is not included in our model.

To investigate mode confinement in a simplified model of the steelpan, we performed two numerical experiments. In the first part of our analysis, we consider how the strength of localization near a note varies with the pan geometry. In the second part, we test the predictions of the landscape theory developed in §2. In each case, the modes of the structure are computed by numerically solving the eigenvalue problem (33) using the finite element method as described in §4(a). Since the localized modes under consideration are insensitive to boundary conditions, we restrict the analysis to shells with a fully clamped boundary. In all cases, we use a triangular mesh, with the mesh size chosen so that the modes of interest have adequately converged; the number of elements is ~ 15000 . We take the constant thickness of the shell to be $h = 1$ mm, which is commonly used for these instruments. In our simulations, we fix the radius of the pan at $R_{\text{pan}} = 0.3$ m, approximately the radius of a traditional steelpan. The material properties are $Y = 200$ GPa, $\sigma = 0.3$ and $\rho = 7850$ kg/m³, typical for mild steel.

In the first experiment, we consider how the localization strength varies with the note and bowl curvatures. For simplicity, we consider a radially symmetric geometry with a single note in the center, shown in figure 3a. The shape is chosen so that the inner note region and outer bowl regions each have constant Gaussian curvature, which we define as κ_i^2 and κ_o^2 respectively. Specifically, the inner note region $0 \leq r < a$ and outer bowl region $b < r \leq 1$ are segments of spheres with radii $R_i = \kappa_i^{-1}$ and $R_o = \kappa_o^{-1}$ respectively (figure 3b). In the transition region $a < r < b$ we choose a smooth interpolation between the inner and outer spherical segments to ensure that the curvature is everywhere defined and continuous. In our experiments, we take $a = 0.05$ m, $b = 0.06$ m, so that the note area is less than 5% of the total area of the pan. As we vary the curvatures κ_i and κ_o , we use two different measures to quantify the localization strength of the so-called (0, 0) mode, which has

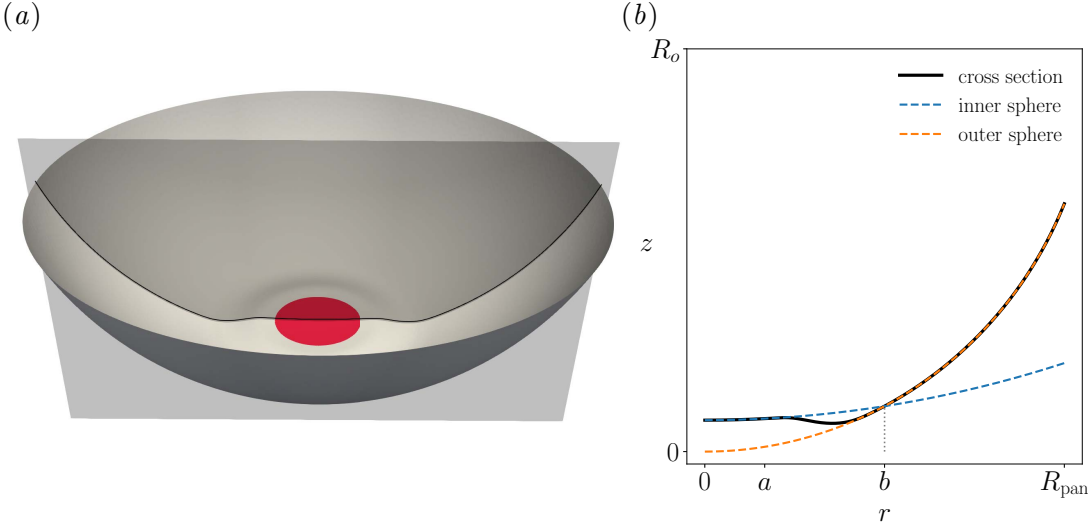


FIG. 3. (a) The idealized steelpan geometry with the diameter of the note indicated. (b) Cross section of an idealized steelpan geometry which smoothly interpolates between an inner sphere of radius R_i for $r \leq a$ and an outer sphere of radius R_o for $r \geq b$. The width $b - a$ of the transition region is exaggerated for clarity.

no nodal lines (see figure 4b). The first is the inverse participation ratio (IPR), which for a mode $u = (\mathbf{u}, \theta)$ of the Naghdi shell is defined by

$$\text{IPR} := \text{area}(\mathcal{S}) \int \|\mathbf{u}\|^4 \, dS \left(\int \|\mathbf{u}\|^2 \, dS \right)^{-2}. \quad (37)$$

If $\|\mathbf{u}\|$ is approximately constant on a subregion $\mathcal{D} \subset \mathcal{S}$ and vanishing outside of \mathcal{D} , then the participation ratio is $\text{area}(\mathcal{S}) / \text{area}(\mathcal{D})$. We also use another, somewhat ad hoc measure of localization, which measures the proportion of the mode that lives in the note region \mathcal{N} in an L^1 -norm sense. If we assume that the mode has been normalized so that $\|\mathbf{u}\|$ has L^1 -norm 1, then this is simply

$$\|\mathbf{u}\|_{L^1(\mathcal{N})} := \int_{\mathcal{N}} \|\mathbf{u}\| \, dA. \quad (38)$$

We refer to this measure as the L^1 -norm ratio (LNR). We note that while the LNR is bounded above by 1 (achieved by any mode that vanishes outside \mathcal{N}), the IPR can be arbitrarily large. These two measures of localization strength are complimentary: The LNR is more sensitive to small amplitude oscillations outside of the note region, but unlike the IPR, it gives no information about how narrowly peaked the mode is inside of \mathcal{N} .

In the second experiment, we use the vector landscape of §2 to study mode confinement in two idealized steelpan geometries, each consisting of a hemispherical bowl with one or more flat note regions where the curvature vanishes. The (nondimensionalized) Gaussian curvature of the bowl is $(h\kappa_o)^2 = 8.2 \cdot 10^{-4}$ in both cases. The first pan shape, depicted in the top left of figure 5a, has a single, circular note of radius 0.05 m in the center. The second geometry, which more closely resembles the elaborate designs of real steelpan instruments, has four notes. Three of those are elliptical inner notes of varying size and eccentricity, placed close together near the center. The fourth note is an approximately rectangular outer note near the boundary (figure 5b). For each of the two pan shapes, we compute the vector landscape \mathcal{L} and several low-frequency eigenmodes. To compute the value of \mathcal{L} at a point y on the shell, we solve the Dirichlet problem $L\mathbf{G}(\cdot, y) = \delta_y I$ for $\mathbf{G}(\cdot, y)$ using the finite element method and compute the integral in equation (13).

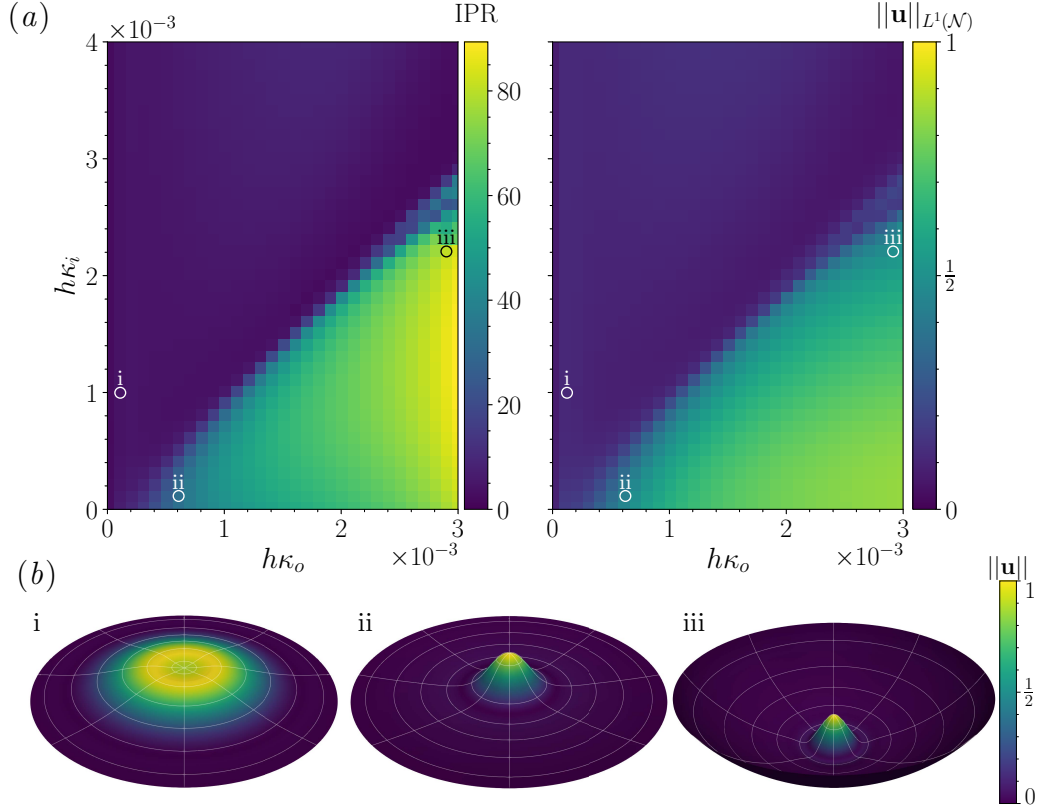


FIG. 4. (a) Inverse participation ratio (left) and L^1 -norm ratio (right) of the $(0, 0)$ mode as a function of the nondimensionalized note and bowl curvatures. A sharp transition from localized to extended modes is seen near the diagonal $\kappa_o = \kappa_i$. (b) Representative mode shapes corresponding to the points marked in (a). Color indicates the normalized displacement and grid lines are shown for clarity. While modes ii and iii have approximately the same L^1 -norm ratio, the latter has a much larger inverse participation ratio.

5. RESULTS

(a) Effect of geometry on mode localization

Figure 4a shows the IPR and LNR of the $(0, 0)$ mode as a function of the bowl and note curvatures. In the region $\kappa_i > \kappa_o$, both localization measures are small and approximately constant, indicating that the mode is extended over most of the pan. Near the diagonal $\kappa_i = \kappa_o$, there is a sharp transition from extended to localized modes which is reflected in both the IPR and LNR. Three representative mode shapes, corresponding to the indicated points i-iii in parameter space, are shown in figure 4b.

In the localized region, $\kappa_i < \kappa_o$, the two localization measures diverge. The L^1 -norm ratio seems to increase monotonically with the difference $\kappa_o - \kappa_i$ between the outer and inner curvatures. The IPR, in contrast, is approximately independent of κ_i in this region, but increases with κ_o . This difference can be seen by comparing modes ii and iii in figure 4b, which are both confined to the note region with similar L^1 norm ratios, but have substantially different values of the IPR. Therefore, the inverse participation ratio gives more fine-grained information about the shape of the localized mode in the note region.

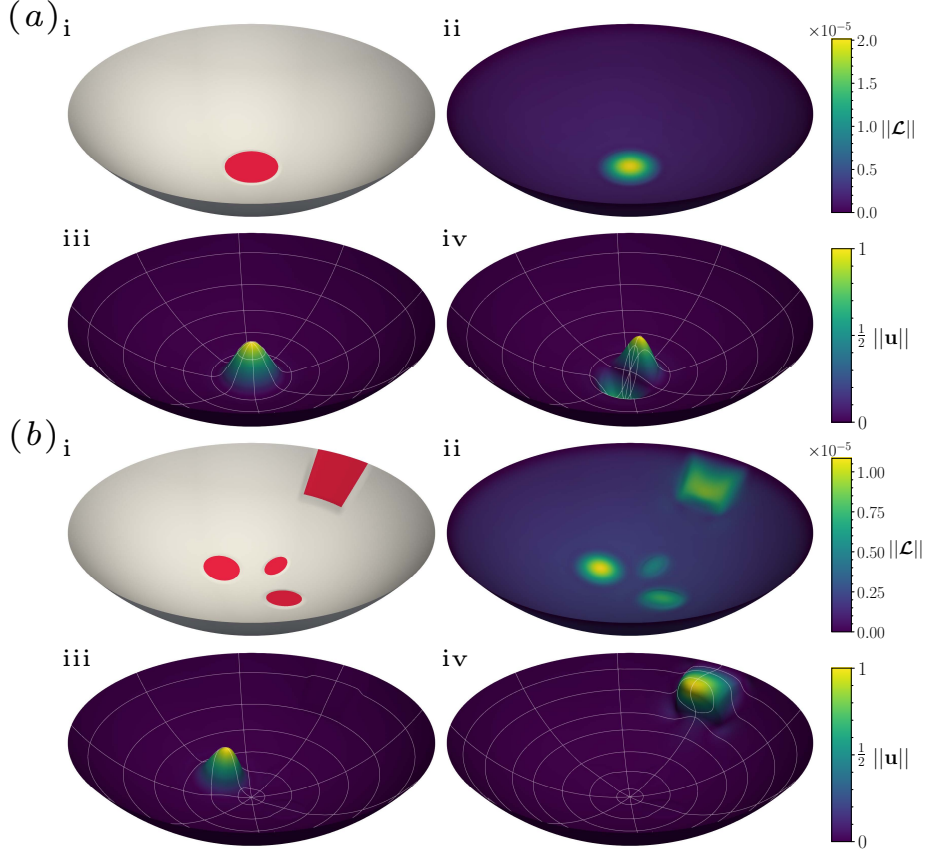


FIG. 5. The vector landscape and several eigenmodes were numerically computed for two steelpan-like geometries, shown in figures (a,b) i with the flat note regions highlighted in red. Figures (a,b) ii show the norm of the vector landscape \mathcal{L} of equation (13) for the two geometries. The first two numerically computed eigenmodes are shown in iii-iv, exhibiting strong localization to the regions predicted by the vector landscape. Color indicates the normalized displacement (white grid lines are shown for clarity). The geometry in figures (a) has a single circular node in the center with $a = 0.05$ m, $b = 0.06$ m, $R_i = 350$ m (see figure 3). The geometry in (b) has four flat notes $K = 0$: A circular note of radius 0.03 m centered at $(x, y) = (-0.075, 0)$ m; an elliptical note with semi-major axis 0.03 m and eccentricity $\sqrt{2}/2$ centered at $(x, y) = (0.075, 0)$ m; an elliptical note with semi-major axis 0.23 m and eccentricity $\sqrt{2}/2$ centered at $(x, y) = (0, 0.075)$ m; a note in the shape of a polar rectangle defined by $r \geq 0.215$ m, $|\theta| \leq \pi/18$ in polar coordinates. For both geometries, the bowl has radius of curvature $R_o = 0.35$ m.

(b) Illustration of the vector landscape

The vector landscape and several lowest eigenmodes were computed for the two shell geometries described in §4. The results for the single-note pan are shown in figure 5a. The norm $\|\mathcal{L}\|$ of the vector landscape is almost vanishing outside of the note region, where it has a sharp peak. Based on this, we predict that the shell supports one or more localized modes in the note region, and only high-frequency modes can have substantial amplitude in the outer bowl region. This is confirmed in the lower half of figure 5a, which depicts the two lowest-frequency modes of the shell. The pan has several more strongly localized modes which are not shown here.

Figure 5b shows the more interesting case of a steelpan with multiple notes of varying size and shape. The vector landscape $\|\mathcal{L}\|$ has several peaks, each located at note region where the curvature vanishes. The tallest peak coincides with the large, circular inner note, followed by a peak at the

rectangular outer note. As explained in §2, the landscape inequality (14) guarantees that any low-lying modes must be confined to the union of the notes regions. While this is an interesting result, it raises the question of whether the vector landscape has the same predictive power as the scalar landscape, which is much stronger than what is guaranteed by the inequality alone. In fact, we observe that each mode is strongly localized to a *single* note region and that the mode shape is reflected in the shape of the corresponding peak of the landscape. Moreover, the relative heights of the peaks is an indicator of the order in which the localized modes appear. For example, the lowest-frequency mode is localized near the tallest peak of the landscape.

6. CONCLUSIONS

The possibility of creating independent, geometrically tunable localized modes has been utilized by makers of steelpans since the early 20th century, but a general quantitative theory for how geometry can lead to effective localization has so far been missing. Inspired by this spectral problem for the steelpan, we first generalized a recent geometric theory for Anderson localization for linear scalar operators to a vector-valued version. We then used the resulting localization landscape theory to predict the locations and order of localized modes in doubly-curved elastic shells by solving a single Poisson-like problem rather than an eigenvalue problem. Our results show an interesting connection between curvature and mode confinement in doubly curved elastic shells: shells with flat regions separated by regions of positive Gaussian curvature support localized modes, and the strength of localization increases with curvature. It might be pertinent to note that our results are size and material independent, as the geometric theory of elastic shells is only predicated on having a large aspect ratio ($R/h \gg 1$). Thus they apply equally to micro- or nanoscale systems, and are suggestive of applications to high quality resonators [30]. More generally, our generalization of the landscape theory to vector-valued systems opens up applications to a much larger class of systems than previously possible.

ACKNOWLEDGMENTS

We thank the NSF MRSEC 2011754, DMR 1922321, the Henri Seydoux Fund, and the Simons Foundation for partial financial support.

REFERENCES

- [1] T. D. Rossing, D. S. Hampton, and U. J. Hansen, Music from oil drums: The acoustics of the steel pan, *Physics Today* **49**, 24 (1996).
- [2] U. Kronman, *Steel Pan Tuning*, Vol. 20 (Musikmuseet, 1992).
- [3] L. E. Murr, E. Ferreyra, J. G. Maldonado, E. A. Trillo, S. Pappu, C. Kennedy, J. De Alba, M. Posada, D. P. Russell, and J. L. White, Materials science and metallurgy of the caribbean steel drum part i fabrication, deformation phenomena and acoustic fundamentals, *Journal of materials science* **34**, 967 (1999).
- [4] T. D. Rossing, U. J. Hansen, and D. S. Hampton, Vibrational mode shapes in caribbean steelpans. i. tenor and double second, *The Journal of the Acoustical Society of America* **108**, 803 (2000).
- [5] S. Maloney, C. Barlow, and J. Woodhouse, A study of mode confinement in caribbean steel drums, in *15th International Congress on Sound and Vibration, Daejeon, Korea* (2008) pp. 2580–2587.
- [6] A. C. H. Morrison, *Acoustical studies of the steelpan and HANG: Phase-sensitive holography and sound intensity measurements*, Ph.D. thesis, Northern Illinois University (2005).
- [7] B. Copeland, A. Morrison, and T. D. Rossing, Sound radiation from caribbean steelpans, *The Journal of the Acoustical Society of America* **117**, 375 (2005).
- [8] R. Vetter, Double second pan, <https://omeka-s.grinnell.edu/s/MusicalInstruments/page/welcome> (2003), accessed: 01-20-22.

- [9] J. F. M. Scott and J. Woodhouse, Vibration of an elastic strip with varying curvature, *Phil. Trans. R. Soc. A* **339**, 587 (1992).
- [10] S. Shankar, P. Bryde, and L. Mahadevan, Geometric control of topological dynamics in a singing saw, *Proceedings of the National Academy of Sciences* **119**, e2117241119 (2022).
- [11] M. Filoche and S. Mayboroda, Universal mechanism for anderson and weak localization, *Proceedings of the National Academy of Sciences* **109**, 14761 (2012).
- [12] P. W. Anderson, Absence of diffusion in certain random lattices, *Phys. Rev.* **109**, 1492 (1958).
- [13] M. Filoche, M. Piccardo, Y.-R. Wu, C.-K. Li, C. Weisbuch, and S. Mayboroda, Localization landscape theory of disorder in semiconductors. i. theory and modeling, *Physical Review B* **95**, 144204 (2017).
- [14] D. N. Arnold, G. David, D. Jerison, S. Mayboroda, and M. Filoche, Effective confining potential of quantum states in disordered media, *Physical review letters* **116**, 056602 (2016).
- [15] D. N. Arnold, G. David, M. Filoche, D. Jerison, and S. Mayboroda, Computing spectra without solving eigenvalue problems, *SIAM Journal on Scientific Computing* **41**, B69 (2019).
- [16] D. N. Arnold, G. David, M. Filoche, D. Jerison, and S. Mayboroda, Localization of eigenfunctions via an effective potential, *Communications in Partial Differential Equations* **44**, 1186 (2019).
- [17] D. S. Grebenkov and B.-T. Nguyen, Geometrical structure of laplacian eigenfunctions, *siam REVIEW* **55**, 601 (2013).
- [18] H.-C. Grunau and G. Sweers, In any dimension a “clamped plate” with a uniform weight may change sign, *Nonlinear Analysis: Theory, Methods & Applications* **97**, 119 (2014).
- [19] Y. Chalopin, F. Piazza, S. Mayboroda, C. Weisbuch, and M. Filoche, Universality of fold-encoded localized vibrations in enzymes, *Scientific reports* **9**, 1 (2019).
- [20] M. Chipot, *Elliptic Equations: An Introductory Course* (Birkhäuser Basel, Basel, 2009).
- [21] B. Davey, J. Hill, and S. Mayboroda, Fundamental matrices and green matrices for non-homogeneous elliptic systems, *Publ. Mat.* **62**, 537 (2018).
- [22] D. Chapelle and K.-J. Bathe, *The Finite Element Analysis of Shells - Fundamentals* (Springer Berlin Heidelberg, 2011).
- [23] P. M. Naghdi, The theory of shells and plates, in *Handbuch der Physik, Volume VI a-2*, edited by S. Flügge and C. Truesdell (Springer, Berlin, Heidelberg, 1972) pp. 425–640.
- [24] D. Arnold and F. Brezzi, Locking-free finite element methods for shells, *Mathematics of Computation of the American Mathematical Society* **66**, 1 (1997).
- [25] J. S. Hale, M. Brunetti, S. P. A. Bordas, and C. Maurini, Simple and extensible plate and shell finite element models through automatic code generation tools, *Computers & Structures* **209**, 163 (2018).
- [26] V. Hernandez, J. E. Roman, and V. Vidal, Slepce: A scalable and flexible toolkit for the solution of eigenvalue problems, *ACM Transactions on Mathematical Software (TOMS)* **31**, 351 (2005).
- [27] J. S. Hale, M. Brunetti, S. P. Bordas, and C. Maurini, *FEniCS-Shells* (2016).
- [28] M. S. Alnæs, J. Blechta, J. Hake, A. Johansson, B. Kehlet, A. Logg, C. Richardson, J. Ring, M. E. Rognes, and G. N. Wells, The fenics project version 1.5, *Archive of Numerical Software* **3**, [10.11588/ans.2015.100.20553](https://doi.org/10.11588/ans.2015.100.20553) (2015).
- [29] P. Bryde and L. Mahadevan, Supplementary material for “Localization in musical steelpans”, [10.6084/m9.figshare.19567621](https://doi.org/10.6084/m9.figshare.19567621) (2022).
- [30] H. G. Craighead, Nanoelectromechanical systems, *Science* **290**, 1532 (2000).